Loads Induced by Terminal-Shock Boundary-Layer Interaction on Cone-Cylinder Bodies

LARS E. ERICSSON*
Lockheed Missiles and Space Company, Sunnyvale, Calif.

An analysis is described that can define the loads induced by shock-induced separation at high subsonic speeds. The supersonic flow region aft of the cone-cylinder shoulder is terminated by a normal shock that causes the boundary layer to separate. At increasing angle-of-attack the leeward side boundary layer is thickened due to crossflow effects and is more easily separated, resulting in a forward movement of the shock. On the windward side, opposite effects occur, and a negative forebody load is generated. When the angle-of-attack exceeds a critical value, the leeward side boundary layer can nowhere support the shock due to the steepening adverse pressure gradient near the shoulder. As a consequence, complete flow separation occurs on the leeward side with an associated large discontinuous change of the forebody load.

Nomenclature

a = speed of sound, mile/sec
$C_{N\alpha}$ = $dC_N/d\alpha$
c = reference length or cylinder caliber, m
M = Mach number (U/a)
N = normal force, kg[coefficient $C_N = N/(\rho U^2/2)S$]
p = static pressure, kg/m²[coefficient $C_p = (p - p_\infty)/(\rho U^2/2)$]
P = static pressure ratio, $P = (p - p)_\infty/p_{t_\infty}$; $P_\xi = \partial P/\partial\xi$
p_t = total pressure, kg/m²
q = dynamic pressure, $q = \gamma pM^2/2$
R_c = Reynolds number, $R_c = U_\infty c/\nu_\infty$
S = reference area, $\pi c^2/4$
U = vehicle velocity, miles/sec
w = crossflow, miles/sec
x = axial coordinate, m
α = angle-of-attack, rad or deg; α_0 = trim value
γ = specific heat ratio ($\gamma = 1.4$ for air)
Γ = $1 + (\gamma - 1)M^2/2$
δ = boundary-layer thickness, m
δ^* = boundary-layer displacement thickness, m
Δ = incremental difference
θ = body attitude, rad or deg
θ_c = cone half-angle, rad or deg
ν = Prandtl-Meyer expansion angle, rad
ν_∞ = kinematic viscosity of freestream, m²/sec
ξ = dimensionless axial distance from cone-cylinder shoulder, $\xi = x/c$
ρ = density of air, kg sec²/m⁴
φ = azimuth angle, rad

Subscripts

a = attached flow
AC = aerodynamic center
$B.L.$ = due to boundary-layer buildup
c = cone
crit = critical
cyl = cylinder
C = total cylinder load
e = local external flow
LW = leeward
WW = windward
0 = at $\xi = 0$
δ = due to pressure gradient buildup (δ = constant)
s = separated flow or shock wave in separated flow
sh = shock wave in attached flow
1,2 = numbering subscripts
∞ = undisturbed flow

Superscripts

i = induced, e.g., $\Delta^i C_N$ = separation-induced normal force coefficient
1 = self-induced pressure in attached boundary layer after normal shock, e.g., p^1
$\hat{}$ = value downstream of normal shock

Received October 23, 1969; revision received April 9, 1970. The results were obtained in a study conducted at the Lockheed Missiles & Space Company for the George C. Marshall Space Flight Center, NASA, under contract NAS 8-20354.

* Senior Staff Engineer. Associate Fellow AIAA.

Introduction

SLENDER cone-cylinder bodies are usually not expected to cause the aerodynamicist any problems. The only problem arises in a very narrow speed range at high subsonic Mach numbers. At these speeds the normal shock terminating the local supersonic speed region aft of the cone-cylinder shoulder causes boundary-layer separation. When the angle-of-attack is increased above a certain critical value, the separation jumps forward to the cone-cylinder shoulder on the leeward side. The associated discontinuous change of the aerodynamic load is very large.

Statement of Problem

Experimental data obtained by Robertson and Chevalier[1] reveal the following distinct terminal shock characteristics on cone-cylinder bodies: At high subsonic speeds a terminal shock appears downstream of the cone-cylinder shoulder, causing local boundary-layer separation (Fig. 1). When the angle-of-attack α is increased, the leeward side separation jumps forward to the cone-cylinder shoulder. The large discontinuous load change can be appreciated by comparing it with the pressure change when α is increased from zero to 2° for $\theta_c = 20°$. The jump to complete leeward side separation occurs at higher α's the more slender the conical forebody is.

Figure 2 shows another characteristic of the interaction between the terminal shock and the boundary layer. The leeward side shock moves forward of the windward side shock at angle-of-attack, thereby creating a negative cylinder load (Fig. 2, left). This is contrary to the expected effect of the increased leeward side Mach number at angle-of-attack, as an increase of Mach number moves the shock back (Fig. 2, right). When the surface Mach number is increased by increasing the cone angle rather than by increasing α, the expected aft movement of the terminal shock results (Figs. 1 and

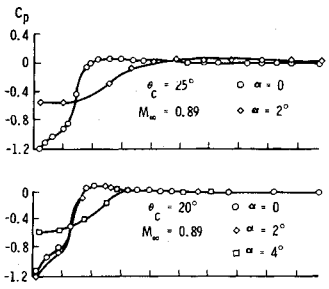

Fig. 1 Effect of angle of attack and cone angle on the aerodynamic characteristics at $M_\infty = 0.89$ of a cone-cylinder body with separated flow (Ref. 1. ξ is distance from cone shoulder).

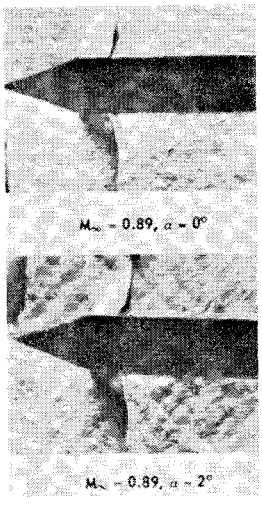

3).† Figure 3 also illustrates the opposite effects of increasing Mach number and increasing angle-of-attack.

The resultant problem may be described as follows. In inviscid flow, the effects of increasing Mach number and increasing angle of attack on the leeward side shock movement would be the same, both causing the shock to move downstream. The forward movement of the leeward side shock and the associated boundary-layer separation in viscous flow results because the leeward side boundary layer is thickened and weakened (profile-wise) through forebody crossflow. Since the unsteady aerodynamic characteristics for inviscid attached flow and for viscous separated flow are drastically different,[3] ability to discriminate between viscous and inviscid effects is essential. In what follows it will be illustrated how this discrimination can be accomplished for cone-cylinder bodies.

Analysis and Discussion of Results

The shock boundary-layer interaction, i.e., the viscous effects on the terminal shock aerodynamics, is governed mainly by how the approaching boundary layer is affected by forebody crossflow and by external axial velocity gradients. The resulting loads are primarily caused by the differential shock locations on leeward and windward sides, and in a first approximation the shock strength can be assumed constant. On the leeward side increasing α produces an increasingly thick boundary layer as well as an increasingly adverse pressure gradient. The consequently weakened boundary-layer

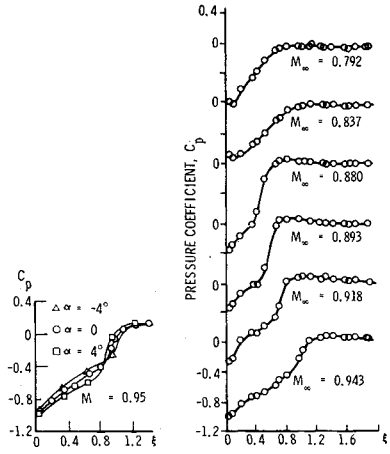

Fig. 2 Effect of α (left) and M_∞ (right) on terminal-shock location on a 20° cone cylinder body.[7]

† The carpet plot[2] as used in Fig. 3 is an invaluable aid in extracting maximum information from experimental results.

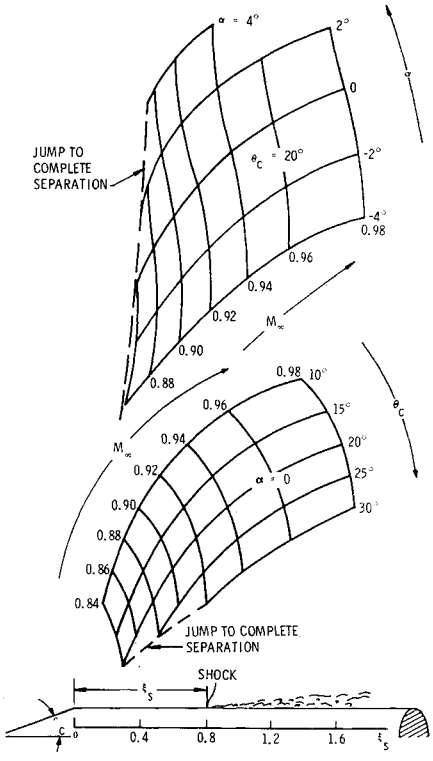

Fig. 3 Combined effects of α, θ_c, and M_∞ on the terminal-shock location on cone-cylinder bodies.

profile cannot negotiate the pressure jump through the shock. The shock, therefore, moves forward to a location where the thinner boundary layer is strong enough to support it (Figs. 2 and 3). In proximity of the cone-cylinder shoulder with the sharply increasing adverse pressure gradient, such an equilibrium position can no longer be found, and the shock jumps all the way forward to the cone-cylinder juncture with a resulting complete leeward-side separation (Fig. 1).

The pressure distributions in Fig. 2 show some slight overpressure behind the shock followed by an expansion down to free-stream pressure p_∞. The overpressure is caused by the separated flow wedge (or flare). In inviscid flow, the pressure aft of the shock would be p_∞, and the pressure distribution could be represented as sketched in Fig. 4. (It will be shown later that the overpressure due to boundary-layer thickening in attached flow can be neglected when determining the shock position.) The pressure distributions in Fig. 2 indicate that the terminal shock is strong and can be treated as a normal shock. Thus, the pressure jump, $p_1/\hat{p}_1 = p_1/p_\infty$, through the shock can be computed using normal shock relations[4]

$$p_1/p_{t_\infty} = p_\infty/p_{t_\infty}\,(p_1/\hat{p}_1)$$

$$(p_1/\hat{p}_1{}^{-1}) = [2\gamma/(\gamma+1)][M_1{}^2 - (\gamma-1)/2\gamma] \qquad (1)$$

$$M_1{}^2 = \Gamma_\infty/\gamma[M_\infty{}^2 - (\gamma-1)/2\gamma]$$

that is,

$$P_1 = (p_1 - p_\infty)/p_{t_\infty} = -(p_\infty/p_{t_\infty})(1 - p_1/\hat{p}_1)$$

$$P_1 = -[2\gamma/(\gamma+1)](1 - M_\infty{}^2)\Gamma_\infty{}^{-\gamma/(\gamma-1)} \qquad (2)$$

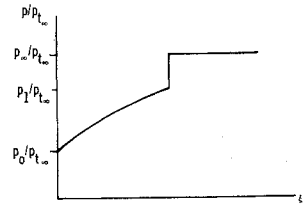

Fig. 4 Sketch of inviscid terminal-shock aerodynamics.

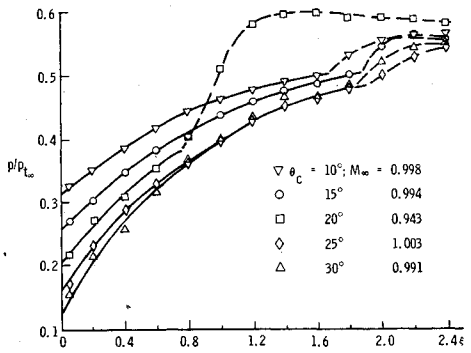

Fig. 5 Transonic pressure distributions over cone-cylinder bodies at $\alpha = 0$ (Ref. 1).

If the inviscid pressure distribution $P(\xi)$ ahead of the shock were known, the terminal shock location ξ_{sh} in inviscid flow would be determined by

$$P(\xi_{sh}) = P_1 \tag{3}$$

Static data for cone-cylinder bodies at high subsonic and transonic speeds[1] show the $P(\xi)$-distributions for various cone angles to be very similar (Fig. 5). Borrowing Syvertson's and Dennis' concept[5] of exponential decay from the shoulder pressure parameter P_0, one may express $P(\xi)$ as follows:

$$P = P_0 e^{(\partial P/\partial \xi)_0 \xi / P_0} \tag{4}$$

Defining $(\partial P/\partial \xi)_0$ as

$$(\partial P/\partial \xi)_0 = -P_0/\xi_0 \tag{5}$$

makes $P(\xi)$ take the following simple form

$$P(\xi) = P_0 e^{-\xi/\xi_0} \tag{6}$$

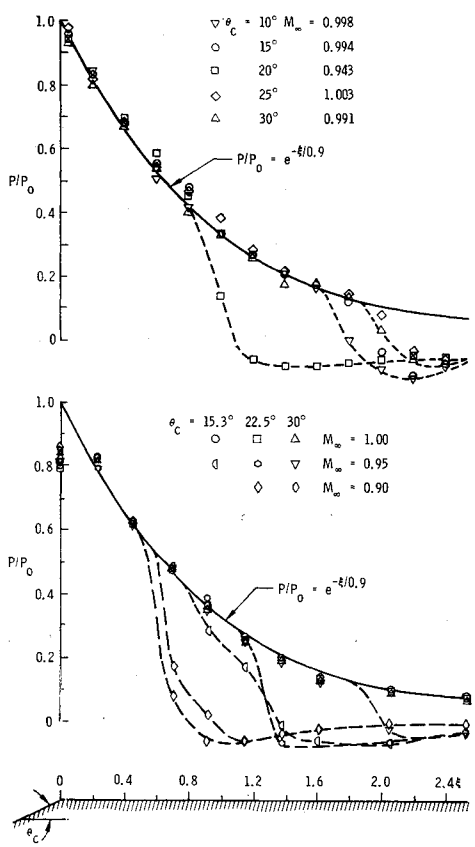

Fig. 6 Effects of θ_c (top) and M_∞ (bottom) on pressure decay $P(\xi)$ from shoulder pressure parameter P_0 at $\alpha = 0$.

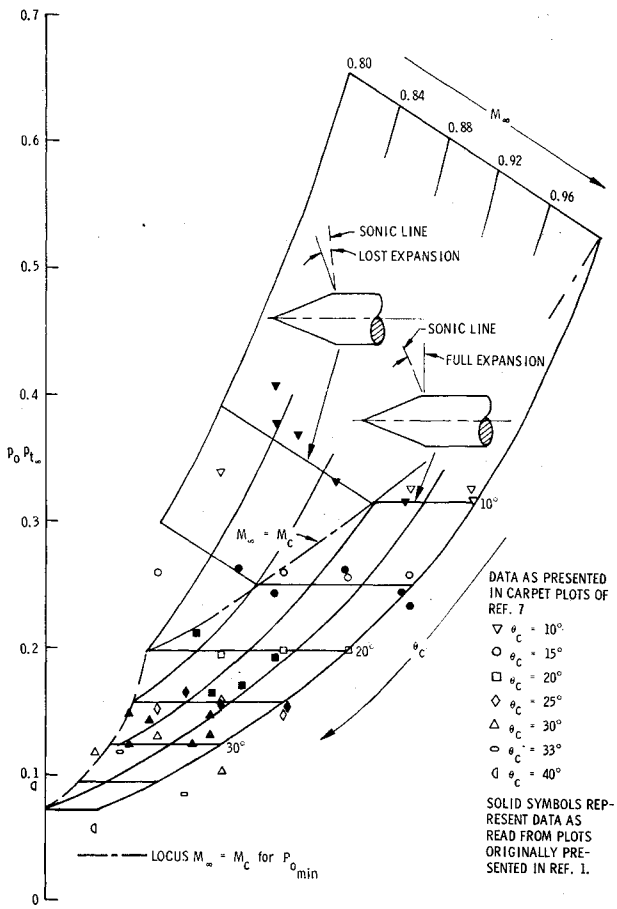

Fig. 7 Shoulder pressure ratio p_0/p_{t_∞} as a function of cone angle θ_c and Mach number M_∞ at $\alpha = 0$.

That is, $P(\xi)$ is determined uniquely by the two parameters P_0 and ξ_0. The pressure distributions in Fig. 5 (Ref. 1) are well correlated by one ξ_0-value (Fig. 6). Also the data obtained at lower Mach numbers and by other investigators indicate that $P(\xi)$ is satisfactorily given by Eq. (6) using a value of $\xi_0 = 0.9$ independent of θ_c and M_∞ (Fig. 6, bottom).‡

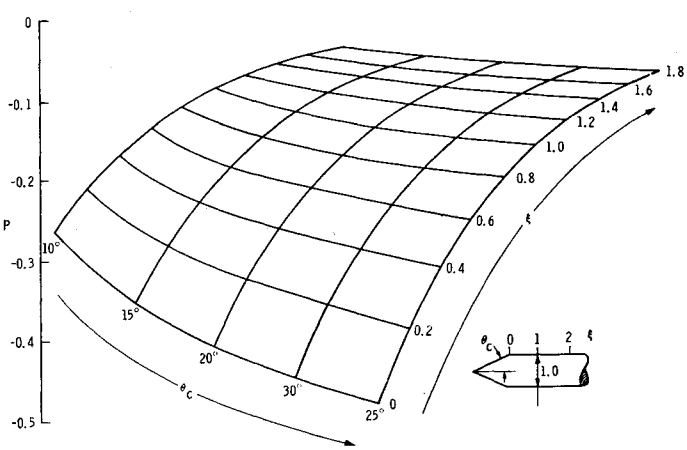

Fig. 8 Inviscid pressure distribution $P(\xi)$ at $M_\infty = 0.88$ and $\alpha = 0$.

‡ The experimental pressures at $\xi = 0$ in the bottom graph of Fig. 6 have not reached their peak values. P^0/p_{t_∞} can only be obtained theoretically, or by extrapolating down to $\xi = 0$, due to the "viscous fairing" of the shoulder.

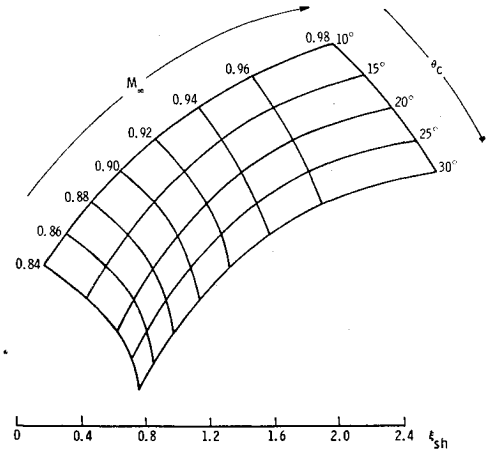

Fig. 9 Combined effect of Mach number and cone angle on the terminal-shock location in inviscid flow over cone-cylinder bodies at $\alpha = 0$.

Combining Eqs. (3) and (6) gives the shock location ξ_{sh} in inviscid flow

$$(\xi_{sh})_{inviscid} = \xi_0 \ln(P_0/P_1) \tag{7}$$

P_1 is given by Eq. (2) and P_0 is obtained through p_0/p_{t_∞} as is shown in Fig. 7, where p_0/p_{t_∞} is given in form of a carpet plot.[2] At slightly higher than critical Mach numbers, $M_\infty \geqq M_{crit}$, sonic speed is reached just before the shoulder expansion, and p_0/p_{t_∞} is well approximated by a 90% effective Prandtl-Meyer expansion. At lower Mach numbers, $M_\infty < M_{crit}$, the pressure drop through the shoulder expansion remains approximately constant. At higher Mach numbers, $M_\infty > M_{crit}$, supersonic cone surface Mach number $M_c > 1$ is reached before the corner, corresponding to an initial (pre-corner) expansion angle ν_0. Thus, P_0 can be described as follows:

$$P_0 \approx \begin{cases} p_0/p_{t_\infty} - p_\infty/p_{t_\infty}; & M_\infty \geq M_{crit} \\ (P_0)_{M_\infty = M_{crit}} \quad ; & M_\infty < M_{crit} \end{cases} \tag{8}$$

$$p_0/p_{t_\infty} = (p/p_{t_\infty})_{\nu = 0.9\theta_c + \nu_0}$$

For the low supersonic range, $1 < M_c \leq 2$, the following approximation of p/p_{t_∞} gives less than 3-% error,[6]

$$(p/p_{t_\infty})_{\nu = 0.9\theta_c + \nu_0} \approx 0.528 \exp[-(2.7\theta_c + 3\nu_0)] \tag{9}$$

With P_0 defined by Eqs. (8) and (9), experimental data from Refs. 1 and 7 were plotted in form of $P(\xi)/P_0$ (Fig. 6). As can be seen, one value of $\xi_0(\xi_0 = 0.9)$ in Eq. (6) defines the attached flow pressure decay within the scatter of the experimental data.

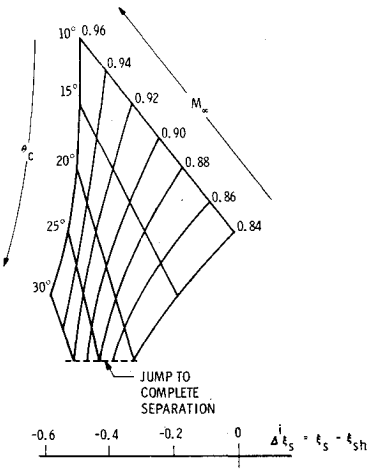

Fig. 10 Effect of boundary-layer separation on terminal-shock location at $\alpha = 0$.

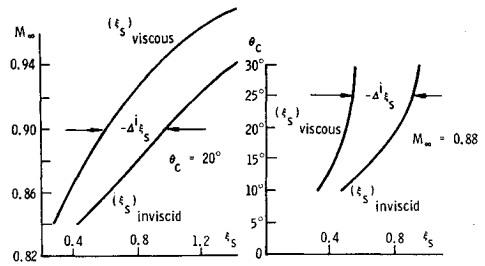

Fig. 11 Terminal-shock location in inviscid and viscous flow on cone-cylinder bodies at $\alpha = 0$.

The inviscid pressure distribution given by Eqs. (6) and (8) for cone-cylinder bodies at $M_\infty = 0.88$ are shown in Fig. 8. The steepening adverse pressure gradient with increasing cone angle is well illustrated. Combining Eqs. (2, 7, and 8) for $\xi_0 = 0.9$ gives the inviscid shock position ξ_{sh} shown in Fig. 9.

In attached flow the boundary-layer displacement slope $\partial\delta^*/\partial x$ would cause the pressure aft of the shock to be $p^1 > p_\infty$. For turbulent boundary layers at Reynolds numbers generally obtained in wind tunnel tests, e.g., those in Ref. 1, the pressure p^1 is at most a few percent above p_∞. Otherwise, by decaying the shoulder pressure exponentially to p^1 instead of p_∞, identically the same shock position as that shown in Fig. 9 would be obtained, regardless of the exact value of p^1.

Because of the boundary-layer shock interaction, the terminal shock location in viscous flow (Fig. 3) is well upstream of the inviscid shock location, as is illustrated in Figs. 10 and 11. The aerodynamic loads produced by the shock-induced boundary-layer separation are determined solely by the terminal shock location on the vehicle.§ As shown in the Appendix, the separation-induced load can be approximated as follows:

$$\Delta^i C_{N\alpha_s} = \Delta C_{ps}[(d\Delta^i\xi_s/d\alpha)_{LW} - (d\Delta^i\xi_s/d\alpha)_{WW}] \tag{10}$$

where ΔC_{ps}, the pressure jump across the shock, is a constant. The shock motion derivative $d\Delta^i\xi_s/d\alpha$ is the difference between the viscous and inviscid motion derivatives, $d\Delta^i\xi_s/d\alpha = d\xi_s/d\alpha - d\xi_{sh}/d\alpha$, where $d\xi_s/d\alpha$ is given by static experimental data (Fig. 3) and $d\xi_{sh}/d\alpha$ can be computed, Eqs. (7)

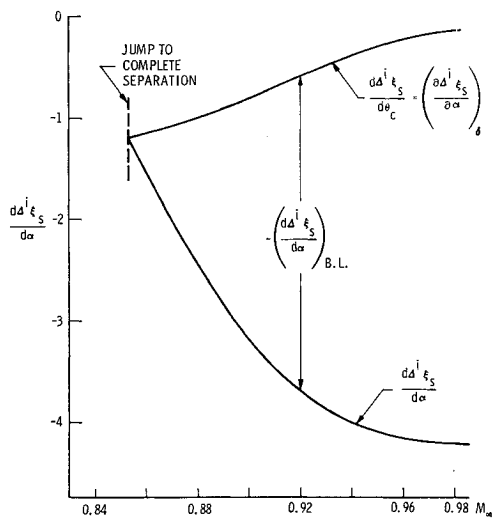

Fig. 12 Effect of boundary-layer thickness and pressure gradient on the terminal-shock movement on a 20 cone-cylinder body at $\alpha = 0$ and high subsonic Mach numbers.

§ This would be true also when including second-order effects due to changing shock strength.

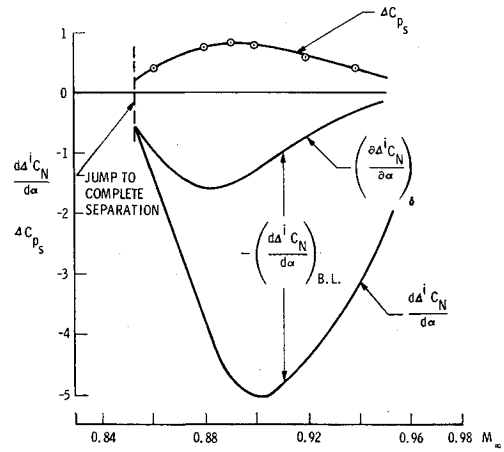

Fig. 13 Normal force derivatives induced by the terminal-shock movement on a 20° cone-cylinder body at $\alpha = 0$ and high subsonic Mach numbers.

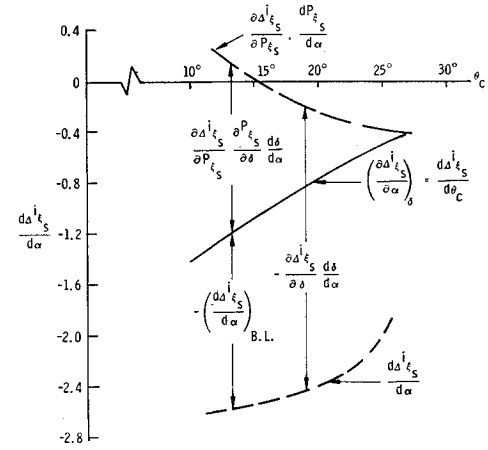

Fig. 15 Decomposition of the angle-of-attack effect $d\Delta^i\xi_s/d\alpha$ into its various components at $\alpha = 0$ and $M_\infty = 0.88$.

and (8). The shock position at angle-of-attack is determined by boundary-layer buildup ($d\delta/d\alpha$) and adverse pressure gradient buildup ($dP_{\xi_s}/d\alpha$). For constant shock strength (see Appendix for justification), the following relations exist:

$$\frac{d\Delta^i\xi_s}{d\alpha} = \frac{\partial\Delta^i\xi_s}{\partial\delta}\frac{d\delta}{d\alpha} + \frac{\partial\Delta^i\xi_s}{\partial P_{\xi_s}}\frac{dP_{\xi_s}}{d\alpha} \tag{11}$$

$$\frac{d\delta}{d\alpha} = \frac{\partial\delta}{\partial w_{AC}}\frac{dw_{AC}}{d\alpha} + \frac{\partial\delta}{dP_{\xi_s}}\frac{dP_{\xi_s}}{d\alpha} \tag{12}$$

$$\frac{dP_{\xi_s}}{d\alpha} = \left(\frac{\partial P_{\xi_s}}{\partial\alpha}\right)_\delta + \frac{\partial P_{\xi_s}}{\partial\delta}\frac{d\delta}{d\alpha} \tag{13}$$

The last term in Eq. (12) can be neglected, as the crossflow effects dominate the boundary-layer buildup. w_{AC} is the crossflow at the aerodynamic center of the body upstream of the shock position, i.e., the forebody crossflow effects are lumped in the manner described in Ref. 3.

Under those assumptions, Eqs. (11–13) define the components $(d\Delta^i\xi_s/d\alpha)_{BL}$ due to boundary-layer buildup at constant inviscid pressure gradient as follows:

$$\left(\frac{d\Delta^i\xi_s}{d\alpha}\right)_{B.L.} = \left(\frac{\partial\Delta^i\xi_s}{\partial\delta} + \frac{\partial\Delta^i\xi_s}{\partial P_{\xi_s}}\frac{\partial P_{\xi_s}}{\partial\delta}\right)\frac{\partial\delta}{\partial w_{AC}}\frac{dw_{AC}}{d\alpha} \tag{14}$$

The component due to (inviscid) pressure gradient increase is

$$\left(\frac{\partial\Delta^i\xi_s}{\partial\alpha}\right)_\delta = \left(\frac{\partial P_{\xi_s}}{\partial\alpha}\right)_\delta \frac{\partial\Delta^i\xi_s}{\partial P_{\xi_s}} \tag{15}$$

In the first approximation, the effect of α without boundary-layer buildup is equivalent to the effect of θ_c (both effects given by a 90-% effective Prandtl-Meyer expansion), i.e.,

$$\left(\frac{\partial\Delta^i\xi_s}{\partial\alpha}\right)_\delta = \frac{d\Delta^i\xi_s}{d\theta_c} = \frac{d\xi_s}{d\theta_c} - \frac{d\xi_{sh}}{d\theta_c} \tag{16}$$

The boundary-layer buildup effect makes up the rest of the total angle-of-attack effect, as illustrated in Fig. 12. When the shock moves closer to the cone-cylinder shoulder with decreasing M_∞, the effect of the boundary-layer buildup, $(d\Delta^i\xi_s/d\alpha)_{B.L.}$, decreases. This is the result of the decreased length. Only the forebody portion aft of the shoulder is effective in this buildup, since the shoulder essentially serves as the starting point for a new boundary layer with or without reverse transition from turbulent to laminar boundary layer.[8] At $M_\infty = 0.85$, the boundary-layer buildup effect has disappeared for 20° cone angle (Fig. 12). The force derivative induced by this shock movement is shown in Fig. 13, as obtained by use of the shock pressure jump, given by Fig. 2 and Eq. (10).

The two force components are

$$\left(\frac{\partial\Delta^i C_N}{\partial\alpha}\right)_\delta = \Delta C_{p_s}\left[\left(\frac{\partial\Delta^i\xi_s}{\partial\alpha}\right)_{\delta_{LW}} - \left(\frac{\partial\Delta^i\xi_s}{\partial\alpha}\right)_{\delta_{WW}}\right] \tag{17}$$

$$\left(\frac{d\Delta^i C_N}{d\alpha}\right)_{B.L.} = \Delta C_{p_s}\left[\left(\frac{d\Delta^i\xi_s}{d\alpha}\right)_{B.L.LW} - \left(\frac{d\Delta^i\xi_s}{d\alpha}\right)_{B.L.WW}\right] \tag{18}$$

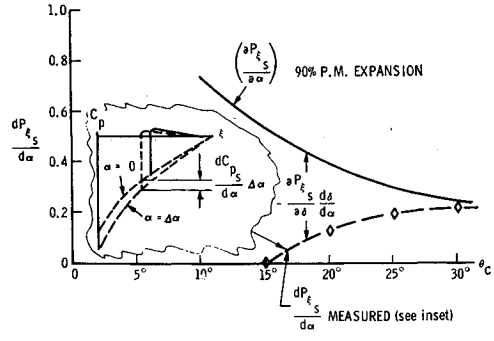

Fig. 14 Effect of angle of attack on adverse pressure gradient at $\alpha = 0$ and $M_\infty = 0.88$.

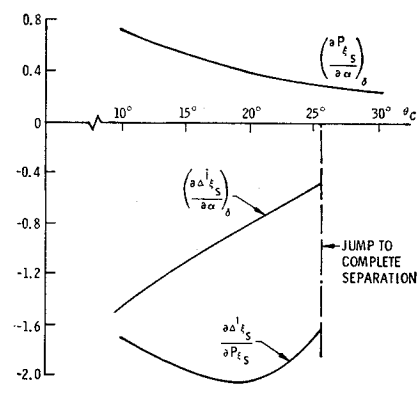

Fig. 16 Effects of adverse pressure gradient at $\alpha = 0$ and $M_\infty = 0.88$.

The pressure gradient immediately ahead of the point of separation (ξ_s), given by Eq. (6), is

$$P_{\xi_s} = (\partial P/\partial \xi)_s = -P_s/\xi_0 \tag{19}$$

Thus,

$$(\partial P_{\xi_s}/\partial \theta_c)_{\text{inviscid}} = -[(P_s/P_0)\partial P_0/\partial \theta_c]/\xi_0 \tag{20a}$$

$$(\partial P_{\xi_s}/\partial \alpha)_{\text{inviscid}} = -[(P_s/P_0)\partial P_0/\partial \alpha]/\xi_0 \tag{20b}$$

Equations (8) and (9) give

$$\partial P_0/\partial \theta_c = -2.7 p_0/p_{t_\infty} \tag{21}$$

Assuming as before that $(\partial P_0/\partial \alpha)_\delta$ is given by $\partial P_0/\partial \theta_c$, one obtains $(\partial P_{\xi_s}/\partial \alpha)_{\text{inviscid}} = (\partial P_{\xi_s}/\partial \alpha)_\delta$ as follows [through Eqs. (20) and (21)]:

$$(\partial P_{\xi_s}/\partial \alpha)_\delta = 2.7(P_s/P_0)p_0/p_{t_\infty}/\xi_0 \tag{22}$$

where

$$P_s/P_0 = C_{p_s}/C_{p_0} \approx -\Delta C_{p_s}/C_{p_{\min}}$$

and

$$p_0/p_{t_\infty} = 0.528 \exp[-(2.7\theta_c + 3\nu_0)]$$

Also, from Eq. (6),

$$P_s/P_0 = \exp(-\xi_s/\xi_0) = \exp(-\xi_s/0.9)$$

Hence,

$$(\partial P_{\xi_s}/\partial \alpha)_\delta = 1.584 \exp[-(1.11\xi_s + 2.7\theta_c + 3\nu_0)] \tag{23}$$

The measured total $dP_{\xi_s}/d\alpha$ may be determined as follows (see sketch in Fig. 14)

$$dP_{\xi_s}/d\alpha = (P_{\xi_s}/C_{p_s})dC_{p_s}/d\alpha \tag{24}$$

where

$$P_{\xi_s} = -(P_s/P_0)P_0/\xi_0 = -1.11P_0 \exp(-1.11\xi_s)$$

For high-cone angles θ_c, the measured effect of α approaches the estimated effect for constant δ (Fig. 14). However, for more slender nose cones, the boundary-layer buildup effect, $(dP_{\xi_s}/d\alpha)_{B.L.}$, has an alleviating influence that at $\theta_c = 15°$ is large enough to cancel completely the inviscid pressure gradient increase with α. Thus, $(d\Delta^i\xi_s/d\alpha)_{B.L.}$ peaks out at $\theta_c = 20°$ (Fig. 15). At lower θ_c it decreases because of the increased $(dP_{\xi_s}/d\alpha)_{B.L.} = (\partial P_{\xi_s}/\partial\delta)(d\delta/d\alpha)$; at higher θ_c it decreases because of the decreasing magnitude of $(\partial\Delta^i\xi_s/\partial\delta)(d\delta/d\alpha)$, resulting when the shock moves closer to the shoulder (as noted earlier in discussing Fig. 12). With $(\partial\Delta^i\xi_s/\partial\alpha)_\delta$ measured as $(d\Delta^i\xi_s/d\theta_c)$, and $(\partial P_{\xi_s}/\partial\alpha)_\delta$ predicted by Eq. (23), the effect of (inviscid) pressure gradient, $\partial\Delta^i\xi_s/\partial P_{\xi_s}$, is given by Eq. (15). The results for $M_\infty = 0.88$ are shown in Fig. 16.

Conclusions

Analytical methods have been developed that can define the loads induced by terminal shock boundary-layer interaction on cone-cylinder bodies at high subsonic speeds. The resulting boundary-layer separation is controlled by forebody crossflow and pressure-gradient adversity. When the shock is not near the cone-cylinder shoulder, the crossflow effects dominate, whereas near the shoulder the adversity of the pressure gradient plays the dominant role. A region exists near the shoulder where the adversity of the pressure gradient is so large that the boundary layer cannot support the normal shock. Consequently, when the angle of attack exceeds a critical value, sudden complete leeward-side separation occurs, and large discontinuous load changes result.

Appendix: Shock-Induced Cylinder Loads

The normal force loading on the cylinder between stations ξ_1 and ξ_t is in coefficient form

$$C_{N_{\text{cyl}}} = -\frac{4}{\pi}\int_{\xi_1}^{\xi_2} 2\int_{-\pi/2}^{\pi/2} C_p(\xi,\varphi)0.5\sin\varphi d\varphi d\xi \tag{A1}$$

The corresponding normal force derivative is

$$(C_{N\alpha})_{\text{cyl}} = -\frac{4/\pi}{q_\infty/p_{t_\infty}}\int_{\xi_1}^{\xi_2}\int_{-\pi/2}^{\pi/2} P_\alpha(\xi,\varphi)\sin\varphi d\varphi d\xi \tag{A2}$$

According to Eqs. (6) and (8),

$$P_\alpha(\xi,\varphi) = \frac{\partial P_0}{\partial\alpha}\exp(-\xi/\xi_0) \tag{A3}$$

p_0/p_{t_∞} is given by Eq. (8) where θ_c now includes the α-effect, i.e.,

$$(\theta_c)_{\text{effective}} = \theta_c + \alpha\sin\varphi \tag{A4}$$

Thus P_α becomes

$$P_\alpha(\xi,\varphi) = -2.7(p_0/p_{t_\infty})\,[\exp(-\xi/\xi_0)]\sin\varphi \tag{A5}$$

and Eq. (A2) gives

$$C_{N\alpha_{\text{cyl}}} = -5.4(p_0/q_\infty)\xi_0[\exp(-\xi_2/\xi_0) - \exp(-\xi_1/\xi_0)] \tag{A6}$$

For a long cylinder, the total cylinder load is ($\xi_2 \to \infty$; $\xi_1 = 0$)

$$C_{N\alpha_C} = 5.4(p_0/q_\infty)\xi_0 \tag{A7}$$

With a terminal shock standing at ξ_{sh} the attached flow pressure jump is, by Eq. (3)

$$\Delta C_{p_{\text{sh}}} = -P_1 p_{t_\infty}/q_\infty \tag{A8}$$

As the shock strength remains constant for M_∞ = constant, P_1 remains constant, and Eqs. (A5) and (A8) give (for $\xi = 0$)

$$d\xi_{\text{sh}}/d\alpha = (\xi_0/P_0)\partial P_0/\partial\alpha = -2.7(\xi_0/P_0)(p_0/p_{t_\infty})\sin\varphi \tag{A9}$$

In the attached flow case, the shock movement can be assumed to vary linearly up to angles-of-attack ($\alpha = \alpha_0 + \theta$) of practical interest ($\alpha \leq 10°$). Thus

$$\left.\begin{aligned} d\xi_{\text{sh}}/d\alpha &= [(d\xi_{\text{sh}}/d\alpha)_{\varphi=\pi/2}]\sin\varphi \\ (d\xi_{\text{sh}}/d\alpha)_{\varphi=\pi/2} &= (d\xi_{\text{sh}}/d\theta)_{LW} = -(d\xi_{\text{sh}}/d\theta)_{WW} \end{aligned}\right\} \tag{A10}$$

The corresponding shock-induced load derivative is obtained through Eq. (A1) as

$$\Delta C_{N\alpha_{\text{sh}}} = 2\Delta C_{p_{\text{sh}}}(d\xi_{\text{sh}}/d\alpha)_{\varphi=\pi/2} \tag{A11}$$

To first order accuracy the total load on the cylinder is

$$(C_{N\alpha_C})_{\text{sh}} = C_{N\alpha_{\text{cyl}}}(\xi_{\text{sh}}) + \Delta C_{N\alpha_{\text{sh}}} \tag{A12}$$

where $\Delta C_{N\alpha_{\text{sh}}}$ is given by Eqs. (A9)–(A11) and $C_{N\alpha_{\text{cyl}}}(\xi_{\text{sh}})$ is obtained from Eq. (A6) with $\xi_2 = \xi_{\text{sh}}$, $\xi_1 = 0$.

Correspondingly, the total cylinder load in separated flow is defined by Eq. (A12) with subscript sh replaced by s. $C_{N\alpha_{\text{cyl}}}(\xi_s)$ is obtained from Eq. (A6) with $\xi_2 = \xi_s$, $\xi_1 = 0$, and $\Delta C_{N\alpha_s}$ is given as

$$\Delta C_{N\alpha_s} = \Delta C_{N\theta_s} = \Delta C_{p_s}\left[\left(\frac{d\xi_s}{d\theta}\right)_{LW} - \left(\frac{d\xi_s}{d\theta}\right)_{WW}\right] \tag{A13}$$

where ΔC_{p_s} is given by Eq. (A8) with subscripts 1 and sh replaced by s. ΔC_{p_s} is assumed to be constant (like $\Delta C_{p_{\text{sh}}}$) and the normal force variation with angle of attack is caused by the shock movement. At nonzero angles of attack the windward-side shock movement becomes small relative to the leeward-side shock movement, and at (trim) angles of attack of moderate magnitudes, e.g., $\alpha_0 \geq 4°$, $(d\xi_s/d\theta)_{WW}$ can be neglected.

The total cylinder forces including shock boundary-layer interaction effects can be expressed as follows:

$$(C_{N\alpha C})_s = C_{N\alpha_{s_1}} + \Delta^i C_{N\alpha_{s_2}} + \Delta^i C_{N\alpha_s} \quad \text{(A14)}$$

$$C_{N\alpha_{s_1}} = 5.4(p_0/p_{t\infty})\xi_0[1 - \exp(-\xi_s/\xi_0)]p_{t\infty}/q_\infty \quad \text{(A15)}$$

$$C_{N\alpha_{s_2}} = 2\Delta C_{p_{sh}}[1 - \exp(-{}^{\Delta^i}\xi_s/\xi_0)]\left(\frac{d\xi_{sh}}{d\alpha}\right)_{LW} \quad \text{(A16)}$$

$$\Delta^i C_{N\alpha_s} = \Delta C_{p_s}[(d\Delta^i\xi_s/d\theta)_{LW} - (d\Delta^i\xi_s/d\theta)_{WW}] \quad \text{(A17)}$$

$$\Delta C_{p_{sh}} = (p_0 - p_\infty)\exp(-\xi_{sh}/\xi_0)/q_\infty \quad \text{(A18)}$$

$$\Delta C_{p_s} = (p_0 - p_\infty)\exp(-\xi_s/\xi_0)/q_\infty \quad \text{(A19)}$$

$$\Delta^i\xi_s = \xi_s - \xi_{sh} \quad \text{(A20)}$$

References

[1] Robertson, J. E. and Chevalier, H. L., "Characteristics of Steady-State Pressures on the Cylindrical Portion of Cone-Cylinder Bodies at Transonic Speeds," TDR 63-104, Aug. 1963, Arnold Engineering Development Center.

[2] Jecmen, D. M., Reding, J. P., and Ericsson, L. E., "An Application of Automatic Carpet Plotting to Wind Tunnel Data Reduction," *Journal of Spacecraft and Rockets*, Vol. 4, No. 3, 1967, pp. 408–410.

[3] Ericsson, L. E. and Reding, J. P., "Analysis of Flow Separation Effects on the Dynamics of a Large Space Booster," *Journal of Spacecraft and Rockets*, Vol. 2, No. 4, Jul-Aug 1965, pp. 481–490.

[4] "Equations, Tables, and Charts for Compressible Flow," Report 1135, 1953, NACA Ames Research Center, Moffett Field, Calif.

[5] Syvertson, C. A. and Dennis, D. H., "A Second-Order Shock-Expansion Method Applicable to Bodies of Revolution Near Zero Lift," Rept. 1328, 1957, NACA.

[6] Guenther, R. A., private communication, Lockheed Missiles & Space Company, Sunnyvale, Calif.

[7] Hammer, R. L. and Leff, H. D., "Linear Aerodynamic Loads on Cone-Cylinders at Mach Numbers from 0.7 to 2.0," CR-413, March 1966, Lockheed Missiles & Space Company, Huntsville, Ala.

[8] Sternberg, J., "The Transition From a Turbulent to a Laminar Boundary Layer," Rept. 906, May 1964, Ballistic Research Laboratory.